First-principles study of spin-dependent thermoelectric properties of half-metallic Heusler thin films between platinum leads

Denis Comtesse,[1] Benjamin Geisler,[1] Peter Entel,[1] Peter Kratzer,[1] and László Szunyogh[2]

[1]*Faculty of Physics, University of Duisburg-Essen and CENIDE, D-47048 Duisburg, Germany*

[2]*Budapest University of Technology and Economics, Department of Theoretical Physics and Condensed Matter Research Group of the Hungarian Academy of Sciences, Budafoki út. 8, H-1111 Budapest, Hungary*

The electronic and magnetic bulk properties of half-metallic Heusler alloys such as Co_2FeSi, Co_2FeAl, Co_2MnSi, and Co_2MnAl are investigated by means of *ab initio* calculations in combination with Monte Carlo simulations. The electronic structure is analyzed using the plane-wave code QUANTUM ESPRESSO and the magnetic exchange interactions are determined using the Korringa-Kohn-Rostoker (KKR) method. From the magnetic exchange interactions, the Curie temperature is obtained via Monte Carlo simulations. In addition, electronic transport properties of trilayer systems consisting of two semi-infinite platinum leads and a Heusler layer in-between are obtained from the fully relativistic screened KKR method by employing the Kubo-Greenwood formalism. The focus is on thermoelectric properties, namely, the Seebeck effect and its spin dependence. It turns out that already thin Heusler layers provide highly spin-polarized currents. This is attributed to the recovery of half-metallicity with increasing layer thickness. The absence of electronic states of spin-down electrons around the Fermi level suppresses the contribution of this spin channel to the total conductance, which strongly influences the thermoelectric properties and results in a spin polarization of thermoelectric currents.

I. INTRODUCTION

The question as to how a spin current can be generated and injected into functional devices is of great interest for future technological applications [1]. Recently, spin-dependent phenomena in the field of thermoelectrics raised a discussion about the interplay between spin, charge, and heat currents [2]. For example, there is the possibility that a strong spin dependence of the Seebeck coefficient can be used to generate a spin accumulation by applying a temperature gradient [3]. This spin accumulation could be used to drive spin currents into functional devices. In other words, one is interested in a thermally driven spin current generator.

The ferromagnetic half-metals are promising candidates in this field because they exhibit a 100% spin polarization of the electronic density of states (DOS) at the Fermi level. This means that there is a gap in the DOS of one of the spin channels and it should, in principle, be possible to extract a 100% spin-polarized current out of these materials. Unfortunately, the sensitive dependence of half-metallicity on details such as interfaces and interface defects has up to now hindered a simple generation of currents with high spin polarization from the half-metals [4]. Therefore, theoretical investigations of promising thermoelectric devices which can inject currents of high spin polarization are of great importance and are investigated, for example, in Ref. [5].

In this work, results of *ab initio* simulations of Co-, Fe-, and Mn-based Heusler alloys are reported. These alloys are half-metallic ferromagnets and have already been considered for spintronics applications (see, e.g., Ref. [4]). Structural, electronic, and magnetic properties as well as the Curie temperature of the alloys are determined by combining *ab initio* methods with Monte Carlo simulations. The Curie temperature is of special interest because it is required to be sufficiently high in order to allow the design of devices which keep the ferromagnetic half-metallicity beyond

room temperature. Details of the half-metallic electronic structure are discussed in terms of the symmetry-resolved electronic density of states (DOS) within the e_g and t_{2g} representations.

In addition, *ab initio* calculations of thermoelectric transport properties of Co_2FeAl, Co_2FeSi, Co_2MnAl, and Co_2MnSi with Pt contacts are performed and a strong dependence on layer thickness and composition is found. Furthermore, the contributions of the two spin channels reveal the possibility that spin-polarized currents can be generated by applying a thermal gradient.

The Heusler layer in-between the Pt leads can be considered as an analog to the Cu-Co multilayers investigated by Gravier *et al*. [6]. The authors report interesting spin-dependent electronic and thermoelectric properties such as the magnetoresistance and magnetothermopower. Recently, such systems have been investigated theoretically by means of *ab initio* calculations focusing on the magnetic anisotropy of the Seebeck coefficient [7].

In this work, the role of the nonmagnetic Cu is taken over by Pt that introduces strong spin-orbit coupling and the magnetic Co is replaced by Co-based Heusler alloys which can be placed within the Pt with only a very small lattice mismatch. The usage of the magnetic Heusler alloys leads to far more degrees of freedom to tune the properties of the system.

For the determination of transport properties, a fully relativistic description of the electronic structure within the screened Korringa-Kohn-Rostoker (SKKR) [8] method in combination with the Kubo-Greenwood formalism is employed. This ensures that the spin-orbit coupling introduced by Pt is taken into account. The relativistic spin-projection operator introduced by Lowitzer *et al*. [9] is used to evaluate the spin-dependent contributions. This operator allows the projection of current contributions onto the two spin channels in the relativistic framework.

The main goals of this work are to provide a pure theoretical description of electronic and finite-temperature magnetism of Co-based Heusler alloys and to evaluate the possibility to drive a highly spin-polarized current by applying a thermal gradient to composite Pt-Heusler systems. As it is difficult to grow large crystals of Heusler alloys with perfect $L2_1$ structure, a direct application of such alloys as half-metallic spin injectors is hindered because half-metallicity is suppressed by disorder. It is much easier to grow thin layers of Heusler alloys with perfect $L2_1$ structure. Therefore, if it turns out that a thin film of half-metallic Heusler between two leads already induces a high spin polarization of the current, the systems under consideration here are of special interest. It is shown throughout this paper that exactly this is possible.

The remainder of the paper is organized as follows: First, details of the calculations are described. Special attention is paid to the details of the transport calculations and the modeling of the Pt-Heusler-Pt systems. Subsequently, results of calculations of the electronic structure of the bulk Heusler systems are presented followed by a discussion of the corresponding magnetic exchange interactions and Curie temperatures. Afterwards, a detailed investigation of transport properties and electronic structure of the Pt-Heusler-Pt systems is carried out. In the final section, the results are summarized and the conclusions drawn from the calculations are discussed.

II. TRANSPORT THEORY FORMALISM

The calculation of electronic transport properties is carried out within the linear-response formalism by employing the Kubo-Greenwood formula [10]

$$\sigma_{\mu\nu}(\boldsymbol{r},\boldsymbol{r}') = \frac{\hbar}{\pi N \Omega} \text{Tr}[\hat{J}_\mu G^+(\boldsymbol{r},\boldsymbol{r}',E)\hat{J}_\nu G^-(\boldsymbol{r},\boldsymbol{r}',E)], \quad (1)$$

where $\sigma_{\mu\nu}$ is the conductivity tensor, $\hat{J}$ is the current operator, and G^+ and G^- are the advanced and retarded Green's functions which are obtained from the KKR formalism. The trace is taken in the four-component Dirac space.

The total conductance of a particular device is expressed as

$$g = \int_{S_R} dS \int_{S_L} dS' \, \hat{\boldsymbol{n}} \, \boldsymbol{\sigma}(\boldsymbol{r},\boldsymbol{r}')\hat{\boldsymbol{n}}', \quad (2)$$

where the S and S' are surfaces in the asymptotic region of the leads and $\hat{\boldsymbol{n}}, \hat{\boldsymbol{n}}'$ are the corresponding normal vectors [11]. This means that the transport perpendicular to the Heusler layers is considered.

To distinguish between contributions of the two spin channels, the fully relativistic spin-projection operator [9]

$$\hat{\mathcal{P}}_z^\pm = \frac{1}{2}\left[1 \pm \left(\beta\Sigma_z - \frac{\gamma_5 \hat{p}_z}{mc}\right)\right] \quad (3)$$

is employed to define the spin-projected current operators $\mathcal{J}^\pm = \hat{\mathcal{P}}_z^\pm \hat{J}$ and the spin-current operator $\mathcal{J} = (\hat{\mathcal{P}}_z^+ - \hat{\mathcal{P}}_z^-)\hat{J}$. Therewith, a correlation between a current induced in one lead and the spin-polarized response current in the other lead is determined. From here on, the two spin channels are denoted by $\uparrow$ and $\downarrow$ instead of $\pm$.

The Seebeck coefficient is evaluated using the approach of Sivan and Imry [12] who defined the moments

$$L_n = -\int g(E)(E-\mu)^n \left[\frac{\partial}{\partial E} f(E,\mu,T)\right] dE \quad (4)$$

from which the Seebeck coefficient

$$S = -\frac{1}{eT}\frac{L_1(\mu,T)}{L_0(\mu,T)} \quad (5)$$

can be calculated. Using this approach, two types of spin-dependent thermoelectric quantities can be defined. The first one is obtained by splitting the numerator of Eq. (5) into two additive contributions, which leads to the definition

$$\tilde{S}_\sigma = -\frac{1}{eT}\frac{L_{1,\sigma}(\mu,T)}{L_0(\mu,T)}, \quad \sigma = \uparrow, \downarrow \quad (6)$$

where the quantities $\tilde{S}$ should not be confused with the Seebeck coefficient of a single spin channel.

Results obtained from the definition given in Eq. (6) give insight into how the two spin channels give additive contributions to the total Seebeck coefficient. It allows us to determine which of the both channels is responsible for the major contribution.

Employing the spin-current operator leads to

$$S_{\text{spin}} = -\frac{1}{eT}\frac{L_{1,\uparrow}(\mu,T) - L_{1,\downarrow}(\mu,T)}{L_0(\mu,T)}, \quad (7)$$

which is understood as a measure of how strong a spin accumulation is driven by the thermal gradient. A more detailed description of the evaluation of spin-dependent thermoelectric properties using the relativistic spin-projection operator is given in Ref. [13].

It is important to note that the temperature dependence of the Seebeck coefficient enters the calculation only in the energy derivative of the Fermi-Dirac functions. This implies that the limit of a vanishing temperature gradient is considered in the sense of linear-response theory. In addition, the contributions from collective excitations, in particular magnons, which can be of great importance considering the driven spin accumulation are not included here.

III. COMPUTATIONAL DETAILS

The determination of structural parameters of the bulk material is carried out with QUANTUM ESPRESSO [14], where a relaxation of the volume is performed and tendencies for tetragonal distortions are examined. The generalized gradient approximation (GGA) exchange-correlation functional of Perdew, Burke, and Ernzerhof (PBE) [15] is used because the structural parameters of metals obtained with this functional are in good agreement with experimental data.

Calculations of magnetic exchange parameters are carried out with the SPR-KKR package [16,17]. Therefore, a scalar-relativistic determination of the multiple scattering properties is performed using the PBE functional. The structural parameters obtained from QUANTUM ESPRESSO serve as input for the KKR calculation. Afterwards, the magnetic exchange parameters are calculated from the scattering properties by employing the Liechtenstein formalism [18,19].

The exchange parameters are subsequently used in Monte Carlo (MC) simulations of the classical Heisenberg model to determine the Curie temperature. The exchange interactions are cut off after three lattice constants. This is sufficient because exchange parameters of larger distance are too small to be relevant for the theoretical estimation of the Curie temperature. The simulation box used within the MC simulations includes $10 \times 10 \times 10$ Heusler unit cells.

Calculations of transport properties are carried out using the fully relativistic screened KKR method [8] and the linear-response formalism in the formulation of Baranger and Stone [20] as first implemented by Mavropoulos *et al.* [11]. In order to ensure an accurate determination of the transport properties, more than 90 000 k points within the irreducible wedge of the two-dimensional Brillouin zone are used. The imaginary part is set to 0.0001 Ry and the energy grid for the calculation of the Seebeck coefficient is 0.001 Ry.

IV. DETAILS OF THE TRANSPORT GEOMETRY

A sketch of the geometry used in the transport calculations is shown in Fig. 1. The layer distance at the interface is the average of the layer distance of Pt and of the Heusler alloy. No lattice relaxations in the interface region are included.

Within the SKKR method the system is assumed to be translational invariant in the x and y directions, and in the z direction the system is terminated on both sides by two semi-infinite leads. Due to the two-dimensional translational invariance, a two-dimensional lattice constant a_{2d} is defined
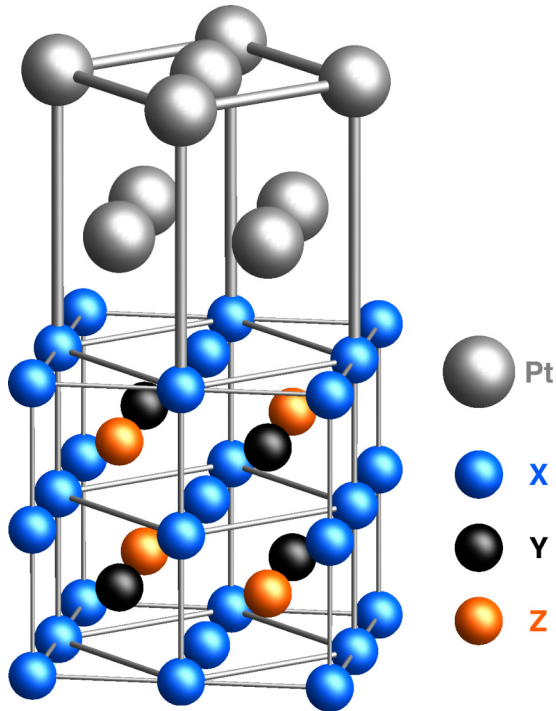

FIG. 1. (Color online) Schematic view of the interface between Pt leads and Heusler layers. The Pt lattice is rotated with respect to the Heusler lattice because the length of the diagonal of the Pt lattice is comparable to the lattice constants of the Heusler alloys. This ensures that the lattice mismatch between both metals is between 0.06 and 0.11 Å.

by

$$a_{2d} = \sqrt{2} a_{bcc}, \tag{8}$$

where $a_{bcc} = a_{3d, Heusler}/2$ is the three-dimensional lattice constant of the underlying bcc lattice of the Heusler part of the system and thus a_{2d} is its diagonal. Hence, the distance between two subsequent Heusler monolayers is given by

$$d = \frac{a_{bcc}}{2} = \frac{\sqrt{2}}{4} a_{2d} . \tag{9}$$

The Pt and the Heusler lattices are rotated by $45°$ with respect to each other. This ensures the smallest possible lattice mismatch between the two structures. For example, the lattice constant of the Heusler cell of Co_2FeSi is 2.81 Å (which is half of the lattice constant of the 16 atoms cell $a_{3d, Heusler}/2$) and the lattice constant of Pt is 3.92 Å. This is of the same order as the diagonal of the Heusler structure is 3.97 Å and therefore close to the Pt lattice constant. This results in a small lattice mismatch between 0.06 to 0.11 Å depending on the particular Heusler alloy.

To simplify the construction of the system, it is assumed that the lattice constant of Pt is the same as that of the two-dimensional lattice constant of the Heusler system:

$$a_{3d, Pt} = a_{2d} . \tag{10}$$

The atomic volume of the Heusler is $a_{bcc}^3/2 = a_{2d}^3/4\sqrt{2}$, hence, the (average) Wigner-Seitz radius is given by

$$\frac{4\pi}{3} R_{WS}^3 = \frac{a_{2d}^3}{4\sqrt{2}} \Rightarrow R_{WS}^H = \frac{1}{4\sqrt[6]{32}} \left(\frac{3}{4\pi} \right)^{1/3} a_{2d}$$
$$\simeq 0.138 \, a_{2d}. \tag{11}$$

In the fcc Pt lattice, the atomic volume is $a_{fcc}^3/4 = a_{2d}^3/4 = 2a_{bcc}^3 = a_{2d}^3/\sqrt{2}$, thus,

$$\frac{4\pi}{3} R_{WS}^3 = \frac{a_{2d}^3}{4} \Rightarrow R_{WS}^{Pt} = \frac{1}{\sqrt[3]{4}} \left(\frac{3}{4\pi} \right)^{1/3} a_{2d}$$
$$\simeq 0.391 \, a_{2d}. \tag{12}$$

Four layers of Pt are included in the interface region to join smoothly to the two semi-infinite bulk regions. The Heusler layer is always terminated by a Co monolayer on both sides. Therefore, the interface between Pt and the Heusler system is always metallic. The distance between the Pt and Co monolayers in the interface is taken to be the average of the Pt and the Heusler interlayer distances, i.e., $(1/2 + \sqrt{2}/4)/2 = (2 + \sqrt{2})/8$. In this way, the atomic radii for all Pt atoms can be taken as R_{WS}^{Pt} and all the atoms in the Heusler alloy can have an atomic radius of R_{WS}^H (H = Heusler) as above, irrespective of their atomic positions.

The assumption of such interface structures between Pt and Heusler alloys turns out to be reasonable because structural relaxation calculations using QUANTUM ESPRESSO do not reveal strong changes. Instead, the relaxations obtained from such configurations are very small. Therefore, it is concluded that the description of the interface chosen here serves as an excellent approximation.

The z axis which points perpendicular to the Heusler layer is chosen to be the quantization axis of the magnetization. This

TABLE I. Lattice parameters and magnetic order obtained from QUANTUM ESPRESSO (GGA) calculations. In addition, the critical temperatures obtained with MC simulations are listed. The experimental value of the critical temperature of Co$_2$FeAl is not known because it is located close to a structural transition.

Composition	Magnetic order	a (Å)	c/a	μ_{tot} (μ_B)	T_C (K)	$T_{C,expt}$ (K)
Co$_2$FeAl	FM	5.70	1	4.99	1050	–
Co$_2$FeSi	FM	5.63	1	5.57	750	1100
Co$_2$MnAl	FM	5.70	1	4.03	510	697
Co$_2$MnSi	FM	5.63	1	5.00	780	985

means that an out-of-plane magnetization is chosen here for all systems under consideration.

V. RESULTS

In the following, a discussion of the electronic structure and the magnetic properties of the bulk systems is given. Afterwards, the transport properties and in particular the Seebeck coefficient of the trilayer systems are presented. The main features found in the calculation of the Seebeck coefficient are subsequently discussed on the basis of the layer-resolved DOS of the trilayers.

At first, the discussion of electronic and magnetic properties of bulk Co$_2$FeAl, Co$_2$FeSi, Co$_2$MnAl, and Co$_2$MnSi is carried out. Table I summarizes structural properties, magnetic moments, and Curie temperatures of all systems under consideration. The magnetic moments are close to the expected integer values [21] except for Co$_2$FeSi, where a significant deviation from the expected 6 μ_B is found. This shows that the *ab initio* description of this particular system is deficient compared to the description of the other half-metallic Heusler systems.

A. Electronic structure

Figure 2 shows the symmetry-resolved electronic density of states of Co and Fe of bulk Co$_2$FeAl. It is apparent that

Co$_2$FeAl is half-metallic because there is a pronounced gap in the minority spin channel and the Fermi energy is located exactly at the upper edge of the gap. The total magnetic moment of 4.99 μ_B shows that the calculation reproduces the expected integer value, revealing only a very small deviation.

Figure 3 shows the symmetry-resolved electronic DOS of Co and Fe in Co$_2$FeSi. There is also a gap in the minority spin channel, but the Fermi energy is not located within this gap but on a shoulder of a peak of the e_g states of Fe. This may be attributed to a deficit of standard GGA concerning the description of the electronic structure of half-metallic Co$_2$FeSi. This has been discussed in more detail in the literature (see, e.g., Ref. [22]). It is argued that strong correlations of the 3d electrons are responsible for this deficit and it is demonstrated that this lack can be cured by employing the LDA+U method. As mentioned above, the DOS in Fig. 3 shows that in particular the description of the e_g states of Fe are deficient because some of the states that should belong to the conduction band leak into the half-metallic gap. In addition, the total magnetic moment of 5.57 μ_B is by more than 0.4 μ_B smaller than the expected integer value of 6.0 μ_B. This problem has to be kept in mind for the interpretation of the later results.

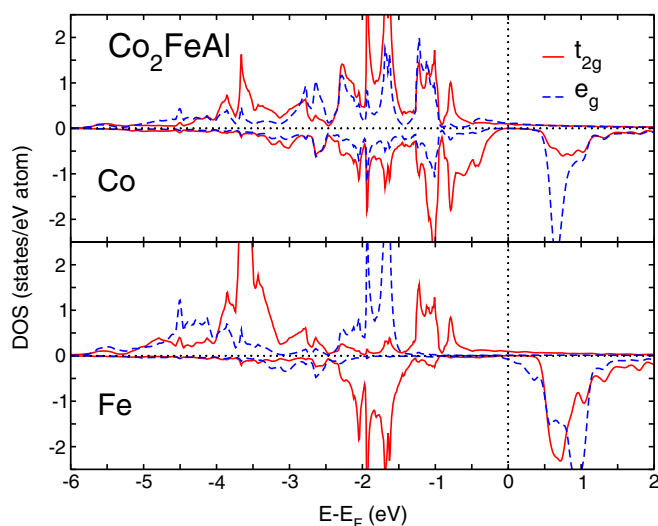In Fig. 4, the symmetry-resolved electronic DOS of Co and Mn in Co$_2$MnAl is shown. There is an obvious gap in the

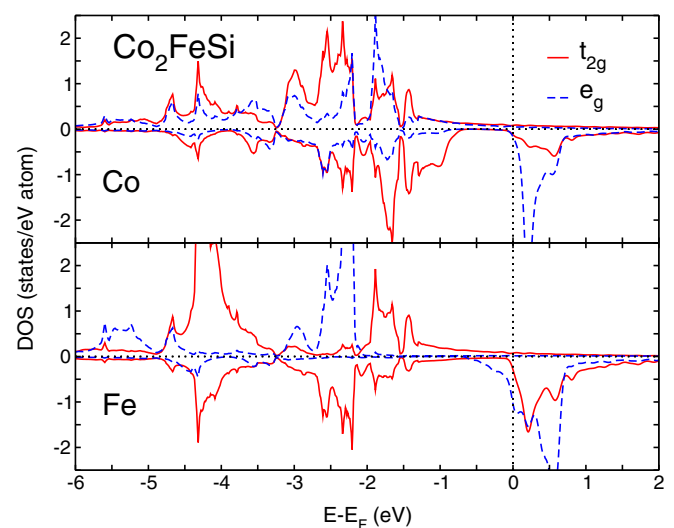FIG. 2. (Color online) Symmetry-resolved electronic density of states of Co and Fe in Co$_2$FeAl. This result shows that there is a gap in the density in the minority spin channel. The Fermi energy lies at the upper edge of this gap.

FIG. 3. (Color online) Symmetry-resolved electronic density of states of Co and Fe in Co$_2$FeSi. Note that this calculation does not reproduce the expected half-metallic behavior. Although there is a gap in the DOS of the minority spin channel, the Fermi energy is not located within the gap.
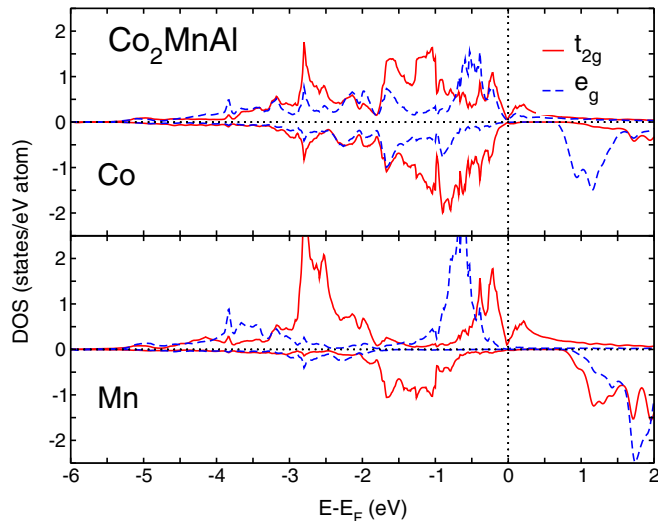
FIG. 4. (Color online) Symmetry-resolved electronic density of states of Co and Mn in Co_2MnAl. There is a pronounced gap in the minority spin channel and the Fermi energy is located at the lower edge of this gap.

minority spin channel, and the calculated magnetic moment is close to the expected integer value. Thus, the GGA description is sufficient in this case and clearly captures the half-metallic properties of Co_2MnAl. The Fermi energy is located at the lower edge of the gap in contrast to the case of Co_2FeAl, where the Fermi energy is located at the upper edge.

Corresponding results of the DOS are shown in Fig. 5 for the case of Co_2MnSi. Again, there is a gap in the minority channel and the Fermi energy is located in the middle of this gap. Therefore, the half-metallicity of Co_2MnSi is very robust against interfering effects such as increasing temperature.

In summary, the electronic structure of all Heusler alloys except Co_2FeSi is in nice agreement with the expected half-
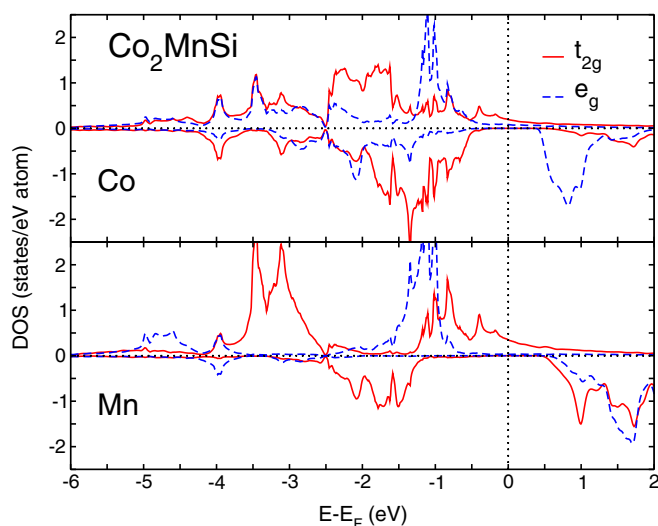
metallic structure. It is found that the location of the Fermi energy within the half-metallic gap depends strongly on the composition. For example, the Fermi level of Co_2FeAl is located at the upper edge of the gap, whereas it is located at the lower edge in Co_2MnAl. Only in Co_2MnSi is the Fermi energy located in the middle of the half-metallic gap. This implies that the conductance of Co_2MnSi in an energy interval around the Fermi level (E_F) is almost exclusively given by the spin-up electrons. Therefore, it is expected that the different locations of the Fermi level affect the thermoelectric properties of the systems.

B. Magnetic properties

In this section, the magnetic exchange parameters and critical temperatures of the Heusler bulk systems are discussed in order to compare between theoretical predictions of T_C and experimentally observed values. Similar investigations are carried out in in Refs. [23,24]. In particular, magnons and spin-stiffness constants are calculated in Ref. [23] from the magnetic exchange interactions, and correlation effects are taken into account by employing the LDA+U method. In Ref. [24], the finite-temperature magnetization of Co_2MnSi is presented as obtained from the random phase approximation.

During the investigation of the calculated magnetic exchange interactions presented here it becomes apparent that the magnetic structure is dominated mainly by the interaction between Co and Fe or between Co and Mn.

The upper panel of Fig. 6 shows the exchange interactions of Co_2FeAl. The most relevant interaction is the one between nearest-neighbor Co and Fe atoms. All other interactions are much smaller and almost negligible. Unfortunately, the predicted critical temperature, which is about 1050 K, can not be compared to experimental values because a structural transition from the ordered $L2_1$ to a disordered $B2$ structure interferes with the temperature region where the magnetic transition is located. This prevents the identification of the exact temperature of the magnetic transition [25]. Nevertheless, the
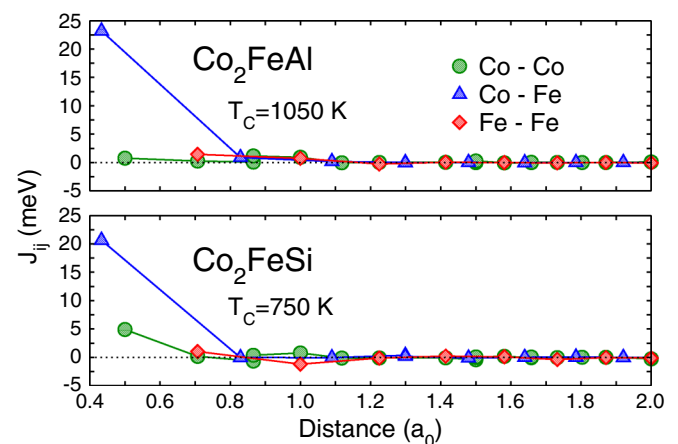

FIG. 6. (Color online) The magnetic exchange parameters and the critical temperature of Co_2FeAl and Co_2FeSi. The strongest contributions to the magnetic exchange interaction of both systems are those of the Co-Fe pairs. All other interactions are small, but in Co_2FeSi the interaction between Co atoms is also noteworthy.

FIG. 5. (Color online) Symmetry-resolved electronic density of states of Co and Mn in Co_2MnSi. There is a pronounced gap in the minority spin channel and the Fermi energy is located in the middle of the gap.

theoretical prediction meets the expected range of the Curie temperature.

In the lower panel of Fig. 6, the magnetic exchange interactions and the Curie temperature of Co_2FeSi are shown. The exchange interactions are qualitatively and quantitatively comparable to those of Co_2FeAl. The most obvious difference is that the Co-Co interactions are stronger in the latter case. The Curie temperature is much smaller than the experimental one. This can be attributed to the incorrect description of the electronic structure within the GGA. As discussed in Sec. V A, an explicit inclusion of correlation effects would improve the description of the electronic structure. Therefore, it is expected that the inclusion of correlations will also improve the description of the exchange parameters and the theoretical prediction of the Curie temperature.

In the following, the Co-Mn-based Heuslers are discussed. Although Mn is known to introduce strong antiferromagnetic interactions, Co_2MnAl and Co_2MnSi are clearly ferromagnets. This can be understood by considering that the antiferromagnetism between Mn pairs has a complicated distance dependence and therefore only pairs which are separated by certain distances interact antiferromagnetically [26].

In Fig. 7, the upper panel shows the exchange interactions and the Curie temperature of Co_2MnAl. The interaction between Co and Mn is now the strongest contribution, although it is by more than a factor of 2 smaller compared to the Co-Fe interaction in Co-Fe-based Heusler systems. The strong Co-Mn interaction is somewhat surprising because in binary CoMn the exchange interaction between nearest-neighbor pairs is usually small, negative, and therefore induces antiferromagnetic coupling. This is understood by considering that the structure of binary $Co_{1-x}Mn_x$ systems is fcc or hcp, and in the Heusler structure Co and Mn atoms are coordinated as in a bcc lattice. This introduces completely different distances.

The lower panel of Fig. 7 shows exchange parameters and critical temperature of Co_2MnSi. Qualitatively, the interactions are again very similar to those of Co_2MnAl. Here, the interactions are stronger and therefore the critical temperature

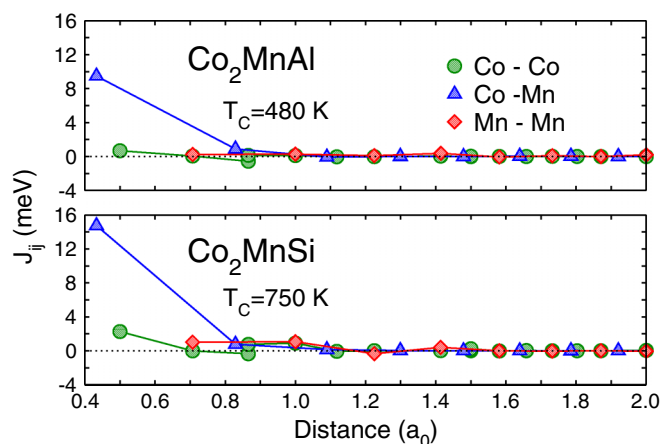is higher compared to Co_2MnAl. As the deviation of the critical temperature from the experimental value is of the same order as for Co_2MnAl, one may conclude that the general trend of the critical temperature is reproduced and the deviations are only due to the systematic errors introduced by the use of the approximative exchange-correlation contributions.

The Curie temperature of Co_2MnSi obtained from the random phase approximation in Ref. [24] gives 964 K, which is very close to the experimental value. In addition, the mean field approximation carried out in Ref. [23] leads to 1011 K, which is also very close to the experiment. This leads to the interesting conclusion that both methods lead to more reasonable results for the Curie temperature compared to the MC simulations in the case of Co_2MnSi. The same is found in the comparison of the mean field value of Co_2MnAl (see again Ref. [23]) and the MC result presented here.

C. Transport properties

In this section, transport properties, in particular the Seebeck coefficient and its spin dependence, of different Pt-Heusler-Pt systems are discussed. For every type of Heusler, systems containing 5 monolayers (ML) are compared to systems containing 9 monolayers of Heusler. The number of monolayers is chosen in a way that the Pt-Heusler interface is purely metallic in the sense that the first Heusler monolayer on both sides contains only Co.

In Fig. 8(a), the calculated temperature dependence of the Seebeck coefficient of Pt-Co_2FeAl-Pt with 5 Heusler monolayers is shown. The Seebeck coefficient increases linearly with temperature. The contribution of the spin-down channel is almost by a factor of 2 larger than the one of the spin-up channel. Figure 9(a) shows the energy dependence of the conductance. Around the Fermi energy, the energy dependence is linear which leads to the linear increase of
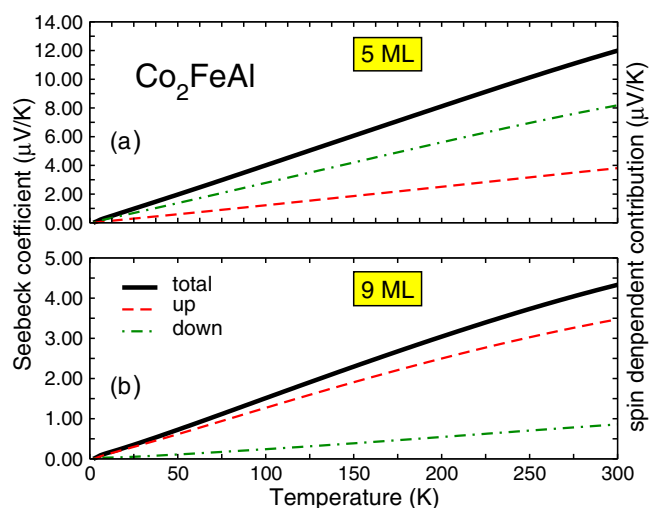

FIG. 7. (Color online) The magnetic exchange parameters and the critical temperature of Co_2MnAl and Co_2MnSi. The dominant contributions are those of the Co-Mn pairs. Comparable to Co_2FeSi, the exchange interaction between Mn atoms in Co_2MnSi is at least remarkable.

FIG. 8. (Color online) Temperature dependence of the Seebeck coefficient of the Pt-Co_2FeAl-Pt system with 5 and 9 monolayers. The black line denotes the total Seebeck coefficient and the green and red lines denote the contributions from the two spin channels according to the color coding used for the energy dependence of the conductance.
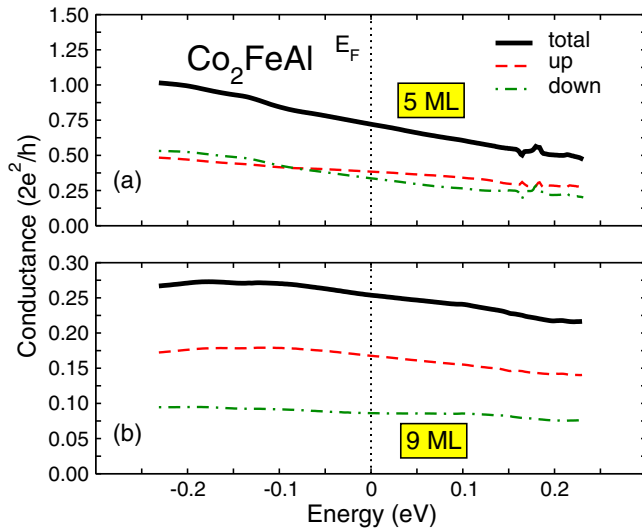
FIG. 9. (Color online) Energy dependence near the Fermi energy of the conductance of the Pt-Co_2FeAl-Pt system with 5 and 9 monolayers. The black line denotes the total conductance, whereas the green and red lines denote the contributions from the two spin channels.

the Seebeck coefficient with increasing temperature. Both spin channels give almost the same contribution to the total conductance, but as the slope of the spin-down part is stronger, its contribution to the Seebeck coefficient is more pronounced.

As shown in Fig. 8(b), the Seebeck coefficient of a system containing 9 monolayers of Co_2FeAl is smaller compared to the system with 5 monolayers. In addition, there is a much larger difference between the contributions of the two spin channels to the total Seebeck coefficient. This can again be explained with the energy dependence of the conductance where the spin-up channel has a slope comparable to that of the total conductance and the energy dependence of the spin-down channel is almost flat. A flat energy dependence leads to small Seebeck coefficients because the slope of this dependence determines the size of the Seebeck coefficient.

The first conclusion that can be drawn from the results for Pt-Co_2FeAl-Pt is that the Seebeck coefficient of the layered system depends strongly on the thickness of the Heusler layer. This basically stems from the different shape of the energy dependence of the conductance. The fact that conductance is very sensitive to the thickness of layers is well known and described, e.g., in Ref. [11]. It is especially interesting that one spin channel can contribute strongly to the total Seebeck coefficient for five layers and gives only a minor contribution for nine layers.

Now, the Pt-Co_2FeSi-Pt systems are discussed. This gives insight into how far compositional changes affect the Seebeck coefficient. In particular, the replacement of Al by Si introduces an additional valence electron. It should also be kept in mind that pure Al is a metal, whereas Si is a semiconductor.

Regarding Fig. 10(a) which shows the temperature dependence of the Seebeck coefficient of a system containing 5 monolayers of Co_2FeSi, it is immediately noticed that the Seebeck coefficient is by more than a factor of 3 smaller compared to the Pt-Co_2FeAl-Pt system with 5 monolayers.
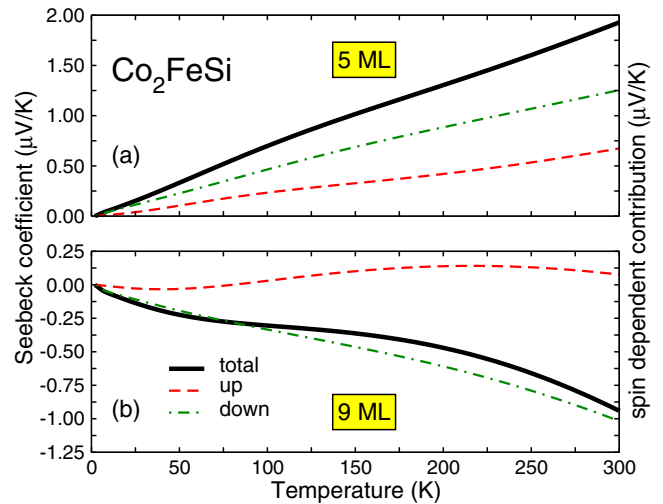

FIG. 10. (Color online) Temperature dependence of the Seebeck coefficient of the Pt-Co_2FeSi-Pt system with 5 and 9 monolayers.

In addition, small deviations from the linear behavior of the Seebeck coefficient are found in this system.

The energy dependence of the conductance shown in Fig. 11(a) is almost linear around E_F but reveals a distinct structure above the Fermi energy and is still quite flat below. There is a pronounced peak above E_F which is connected to numerical inaccuracies that can occur if strong changes of the electronic structure appear during the energy sampling. In such cases, the k-point mesh used within the calculation can be commensurate with important features in the two-dimensional Brillouin zone at a certain energy but can miss some features at another energy. As such structures affect the calculation of the Seebeck coefficient only very weakly, the enormous numerical effort which is required to cure this lack is not necessary.

Turning to the Pt-Co_2FeSi-Pt system with 9 monolayers shown in Fig. 10(b), a strong change occurs in comparison
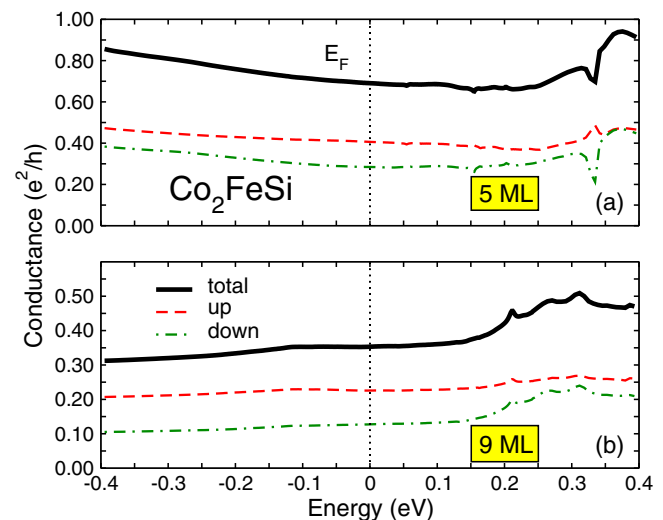

FIG. 11. (Color online) Energy dependence of the conductance of the Pt-Co_2FeSi-Pt system with 5 and 9 monolayers of Heusler around the Fermi energy.

to the system with 5 monolayers. The Seebeck coefficient of this system is negative and the evolution with temperature is not linear as for the systems with 5 monolayers. In addition, the two additive contributions to the total Seebeck coefficient have opposite signs. The contribution of the spin-down channel which gives the strongest contribution is negative, whereas the contribution of the spin-up channel is small and positive. Therefore, the resulting total Seebeck coefficient is very small. This can be understood by considering the energy dependence of the conductance around the Fermi level [see Fig. 11(b)] which is almost flat and therefore gives only small contributions to the Seebeck coefficient. This behavior changes around 0.1 eV away from the Fermi energy when more structure comes into play. However, this structure is again in an energy region which contributes only weakly to the Seebeck coefficient at temperatures up to 300 K.

In a next step, the Y component of the Heusler compound is changed from Fe to Mn. This results in a larger Seebeck coefficient for systems containing 5 monolayers of Co_2MnAl [see Fig. 12(a)]. Here, the additive contributions of the spin channels to the total Seebeck coefficient are almost of the same size and exhibit a comparable structure. The energy dependence of the conductance of this system is shown in Fig. 13(a). It reveals a strong slope of the total conductance and both spin-dependent contributions. The conductance of both spin channels has almost the same slope which result in almost the same contribution to the total Seebeck coefficient. Interestingly, the qualitative shape of the energy dependence of the conductance and its spin-dependent contributions of the Pt-Co_2FeAl-Pt system with 5 monolayers is comparable to that of the Pt-Co_2MnAl-Pt with the same number of layers.

In the system containing 9 monolayers of Co_2MnAl between the Pt leads [see Fig. 12(b)], the total Seebeck coefficient increases. This is contrary to the Co_2FeZ systems where the Seebeck coefficient is smaller in the nine-layer case. But here there is a sizable slope at low temperatures and it seems to saturate for larger temperatures. This saturation stems from the flat regions of the energy dependence of the conductance
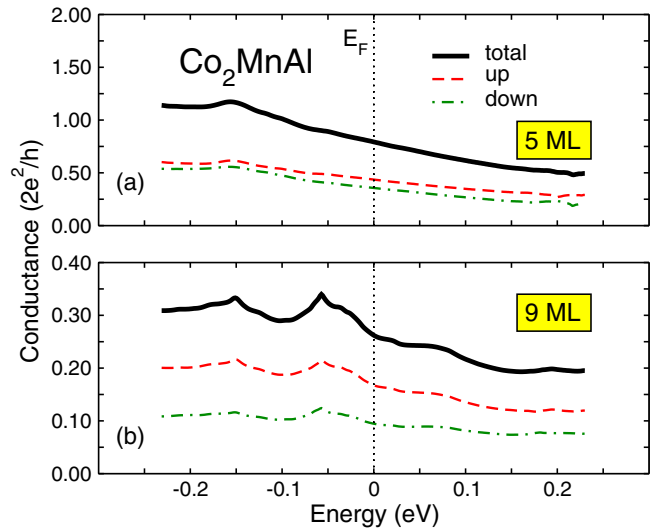

FIG. 13. (Color online) Energy dependence of the conductance of the Pt-Co_2MnAl-Pt system with 5 and 9 monolayers of Heusler around the Fermi energy.

at more than 1.5 eV away from the Fermi energy. Although there is a pronounced structure below the Fermi energy, the average slope in this region is small and therefore this region gives almost no contribution to the Seebeck coefficient. This system is a perfect example of a system with small conductance (speaking in terms of ballistic conductance at the Femi level) but with a large Seebeck coefficient. This shows again that the Seebeck coefficient depends almost exclusively on the slope of the conductance and much less on its absolute value.

To finish the discussion of the transport properties, the Seebeck coefficient of Pt-Co_2MnSi-Pt systems has to be discussed. Figure 14(a) shows its temperature dependence for the system containing 5 monolayers of Heusler. The absolute value is decreased compared to the Pt-Co_2MnAl-Pt system. This is analogous to the decrease found in the Co-Fe-based system where the exchange of Al by Si reduces the Seebeck
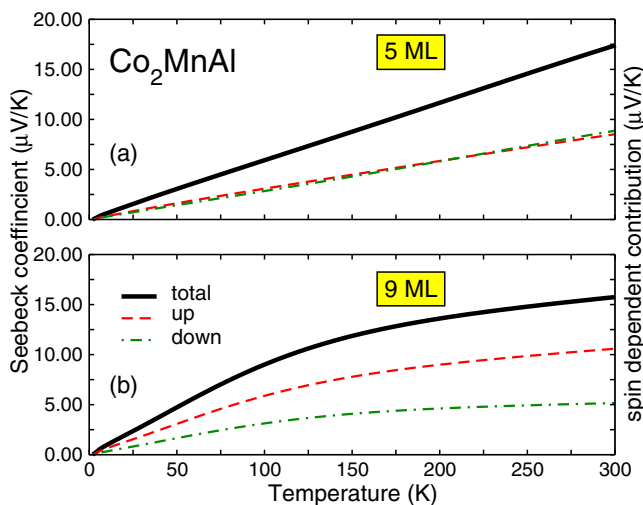

FIG. 12. (Color online) Temperature dependence of the Seebeck coefficient of the Pt-Co_2MnAl-Pt system with 5 and 9 monolayers of Heusler.
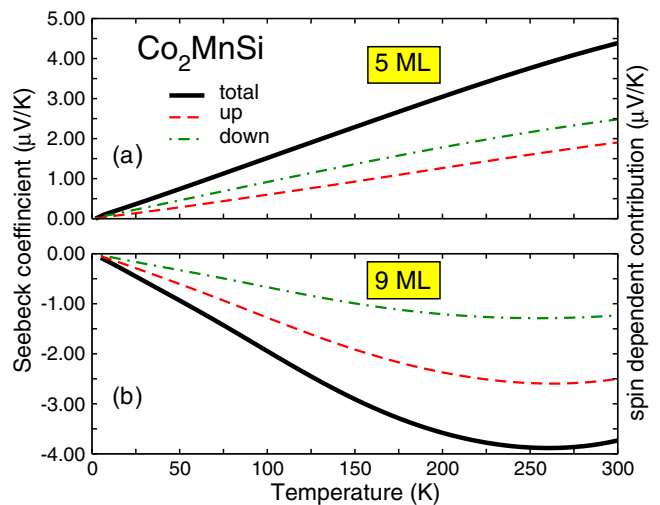

FIG. 14. (Color online) Temperature dependence of the Seebeck coefficient of the Pt-Co_2MnSi-Pt system with 5 and 9 monolayers.
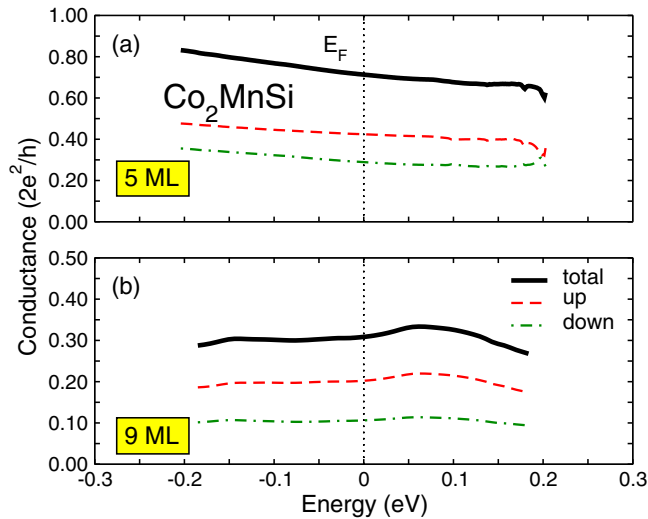
FIG. 15. (Color online) Energy dependence of the conductance of the Pt-Co$_2$MnSi-Pt system with 5 and 9 monolayers of Heusler around the Fermi energy.
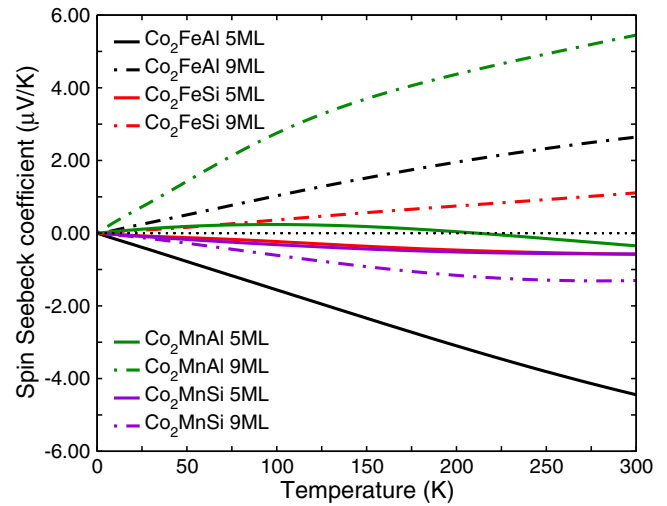

FIG. 16. (Color online) Comparison of the temperature dependence of the spin Seebeck coefficient of all systems under consideration.

coefficient strongly. The evolution of the additive contributions from the spin channels to the total Seebeck coefficient with temperature for Pt-Co$_2$MnSi-Pt is qualitatively comparable with the one of Pt-Co$_2$MnAl-Pt because they are almost of the same size. The energy dependence of the conductance shown in Fig. 15(a) is linear with almost no structure.

The last system that has to be discussed is the system which contains 9 monolayers of Co$_2$MnSi, and its Seebeck coefficient is shown in Fig. 14(b). This system exhibits a very interesting behavior because the Seebeck coefficient is negative and has a minimum at around 275 K.

The energy dependence of the conductance shows a bump above the energy and a flat behavior below. This asymmetry leads to the unusual temperature dependence of the Seebeck coefficient. The slope at energies above the energy of the bump is negative and therefore contributes positive to the Seebeck coefficient. This results in the minimum of the temperature dependence of the Seebeck coefficient.

Table II summarizes the sign of the Seebeck coefficient of all systems studied here. It shows a systematic difference between systems containing Al and those containing Si. All systems containing Al considered here exhibit a positive Seebeck coefficient for both layer thicknesses in combination with Fe and also with Mn. The systems that contain Si show a positive Seebeck coefficient for 5 monolayers of Heusler for the case of Fe and Mn and a negative Seebeck coefficient for 9 monolayers in both combinations with Fe and Mn.

TABLE II. This table summarizes which combination of elements and layer thickness leads to positive or negative Seebeck coefficients.

	Al		Si	
	5 ML	9 ML	5 ML	9 ML
Fe	+	+	+	−
Mn	+	+	+	−

Figure 16 shows the spin Seebeck coefficient defined in Eq. (7) of all systems investigated throughout this section. The systems with 5 monolayers of Co$_2$FeAl and 9 monolayers Co$_2$MnAl lead to the largest effect but in the first case the spin Seebeck coefficient is negative and in the second it is positive. Therefore, the thermoelectric current in this systems exhibits the strongest spin polarization but with opposite sign.

D. Electronic structure of the transport systems

In order to get a deeper insight into how the thermoelectric properties depend on the layer thickness and the composition, the electronic structure of the Pt-Heusler-Pt systems discussed here has to be understood in more detail. Therefore, this section is devoted to the discussion of the electronic DOS of the Heusler layers between Pt leads which has been obtained with QUANTUM ESPRESSO. The main question is if there are signatures of half-metallicity in the small Heusler layers and how they influence the Seebeck coefficient and its spin dependence.

In order to give a more complete overview of the electronic structure of the trilayer system, the DOS of the first three Pt layers of the leads are shown in the Appendix. In Figs. 17 and 18, the electronic DOS of the two Pt-Co$_2$FeAl-Pt systems is shown. The DOS of only the first three and five Heusler layers is presented because the subsequent layers reveal the same DOS because of the reflection symmetry of the system. The upper DOS always corresponds to the Co layer at the interface to the Pt leads. One easily observes that in the system containing only 5 monolayers of Heusler, the half-metallic gap is absent even in the Co layer in the middle. However, the DOS becomes more similar to that of bulk Co$_2$FeAl in the middle of the Heusler layer compared to the DOS in the monolayer which is directly connected to the Pt lead. This shows that the influence of the interface decays very fast.

If the DOS of the system containing 9 monolayers of Co$_2$FeAl is examined, one observes that the half-metallic gap is recovered in the middle of the system. This means that
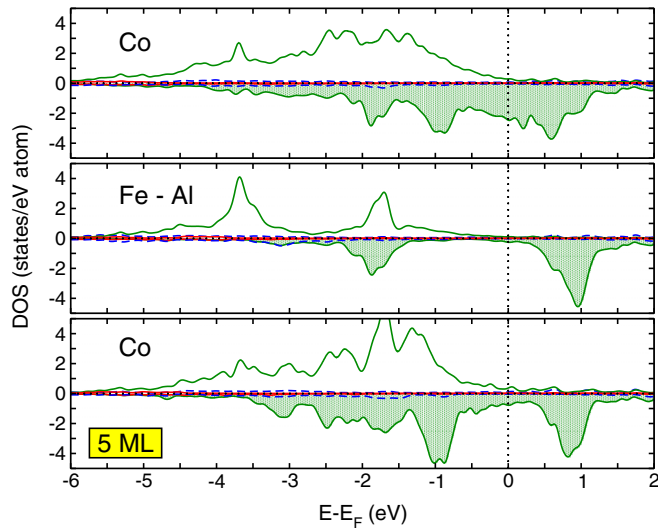
FIG. 17. (Color online) DOS of the Pt-Co$_2$FeAl-Pt system with 5 monolayers of Heusler between the Pt leads. Here and in the following 7 figures, green lines and shaded areas show layer-resolved projections on the 3d orbitals of the denoted layer, while red solid and blue dashed lines depict summed-up projections on the valence s and p orbitals, respectively.

FIG. 19. (Color online) DOS of the Pt-Co$_2$FeSi-Pt system with 5 monolayers of Heusler between the Pt leads.

the influence of the Pt interface is almost completely decayed after four layers. The occurrence of this gap is responsible for certain differences of the Seebeck coefficient between the system with 5 and 9 monolayers.

Comparing the energy-dependent conductances in the upper and lower panel of Fig. 9 to the DOS in Figs. 17 and 18, it becomes obvious why the contribution of the two spin channels is different for different numbers of monolayers. For 5 monolayers, both spin channels give almost the same contribution to the conductance, whereas for 9 layers the contribution of the spin-up channel is almost twice as large. This results from the occurrence of the half-metallic gap in the spin-down
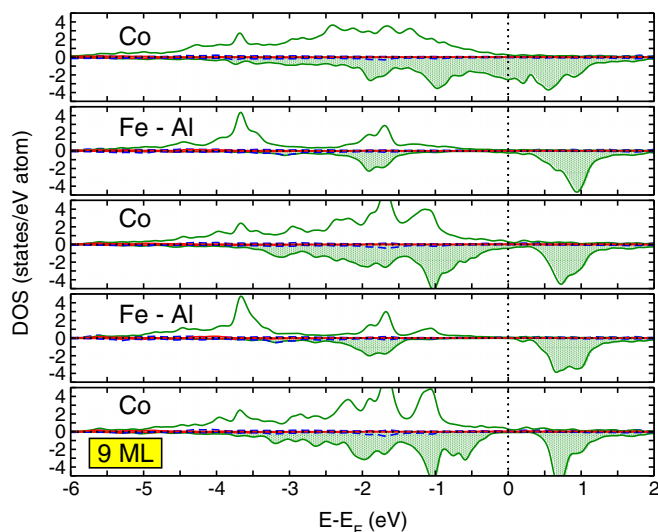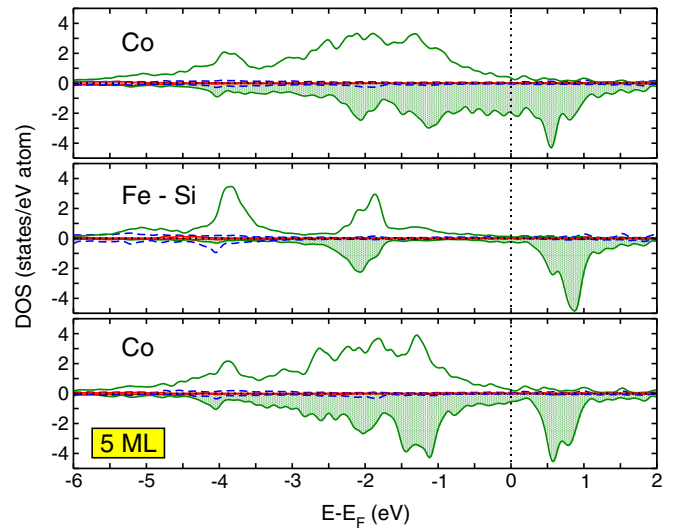
DOS of the system with nine Heusler layers. The absence of states in the spin-down channel in the middle of the system reduces the transmission probability of spin-down electrons significantly. The remaining transmission can be explained by the occurrence of electrons that flipped their spin on the way through the system and by the occurrence of spin-down electrons that tunnel through the small region where there is no spin-down state. The reduction of the total conductance is a general trend observed in all systems. This general thickness dependence can be attributed to the occurrence of interference due to multiple reflection within the Heusler (for detail, see Ref. [11]).

The same arguments are also valid for the Pt-Co$_2$FeSi-Pt systems. Their DOS are shown in Figs. 19 and 20. Again, the occurrence of the gap in the spin-down channel in the nine-layer system leads to a 50% smaller contribution of this
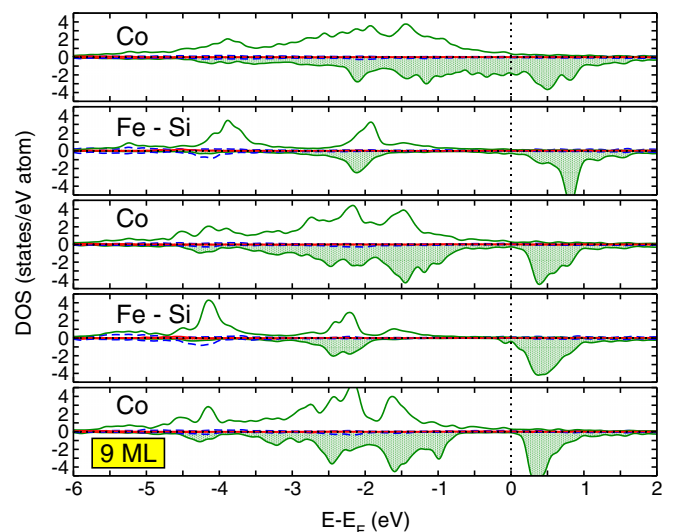

FIG. 18. (Color online) DOS of the Pt-Co$_2$FeAl-Pt system with 9 monolayers of Heusler between the Pt leads.

FIG. 20. (Color online) DOS of the Pt-Co$_2$FeSi-Pt system with 9 monolayers of Heusler between the Pt leads.

FIG. 21. (Color online) DOS of the Pt-Co$_2$MnAl-Pt system with 5 monolayers of Heusler between the Pt leads.
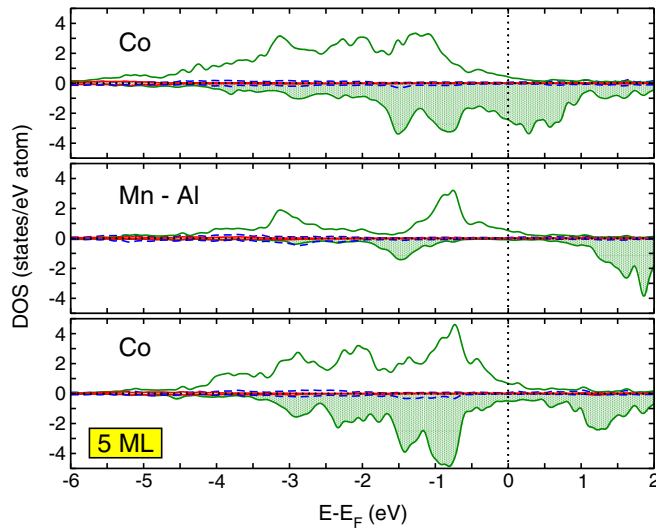

FIG. 22. (Color online) DOS of the Pt-Co$_2$MnAl-Pt system with 9 monolayers of Heusler between the Pt leads.

channel compared to the spin-up channel. The sudden increase of the conductance above the Fermi energy in the nine-layer system can be related to the peak in the DOS above the Fermi energy. The sudden occurrence of states in the middle of the system leads to the occurrence of many new transmission channels. Therefore, the conductance of the spin-down channel increases, which of course leads to an increase of the total conductance.

The energy dependence of the five-layer Pt-Co$_2$MnAl-Pt system is also easily described by features of the DOS which is shown in Fig. 21. The DOS of both spin channels is relatively large at the Fermi energy which leads to the occurrence of many transmission channels and therefore to a quite large conductance. In the nine-layer system (see Fig. 13), the total conductance is again reduced and also the spin-down conductance is again almost a factor of 2 smaller. This is again connected to the occurrence of the half-metallic gap (see Fig. 22).

Concerning the DOS of the Pt-Co$_2$MnSi-Pt systems, the results are similar to those of the other systems (see Figs. 23 and 24). The half-metallic gap is fully recovered in the nine-monolayer system. Therefore, the small conductance contribution of the spin-down channel in this system can be attributed to this feature. Although the Fermi level of this system is almost exactly in the middle of the gap, the conductance is only small but not zero. This shows that there must be enough channels through which electrons can travel from one side to the other tunneling through the monolayers without spin-down states.

The systematic behavior of the sign of the Seebeck coefficient as summarized in Table II can also be related to the features of the electronic DOS. The DOS of the Pt-Co$_2$FeAl-Pt and Pt-Co$_2$MnAl-Pt systems show that the Fermi energy has the tendency to be located closer to the valence edge of the spin-down channel. This is different in Pt-Co$_2$FeSi-Pt and Pt-Co$_2$MnSi-Pt where the Fermi energy shows a tendency for the conduction edge of the spin-down channel. A Fermi energy at the edge of the valence band leads to a large conductance
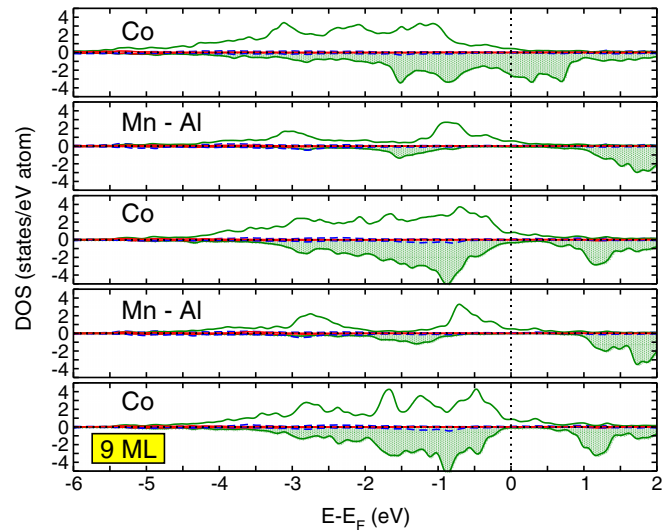
below because of the large number of channels and a Fermi energy at the edge of the conduction band leads to a large conductance above. This has a strong effect on the slope of the energy dependence of the conductance which determines the Seebeck coefficient. A negative slope is connected to a Fermi energy at the valence band and a positive slope to a Fermi energy at the conduction band.

Another summarizing comparison is given in Table III where the polarization of the total DOS at the Fermi energy of the systems is compared to the polarization of the associated conductance. This polarization is defined by $(\uparrow - \downarrow)/(\uparrow + \downarrow)$ where the arrows stand for the actual spin-up or spin-down contribution. The most interesting observation is that the polarization of the DOS is negative for all systems, whereas the polarization of the conductance is always positive. This is connected to a large peak in the minority channel of the total
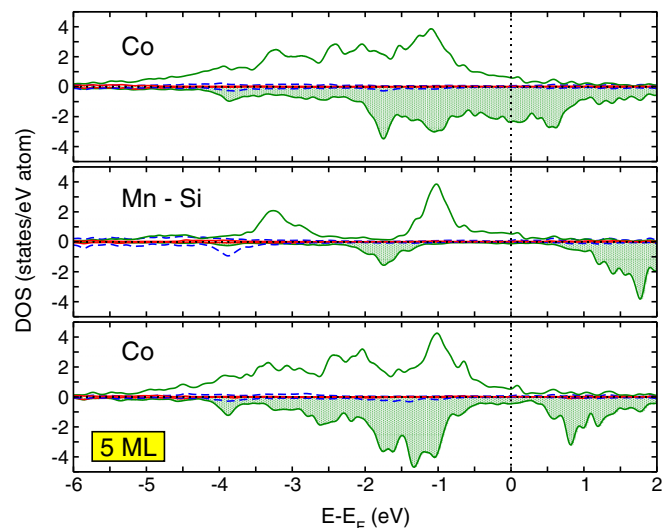

FIG. 23. (Color online) DOS of the Pt-Co$_2$MnSi-Pt system with 5 monolayers of Heusler between the Pt leads.
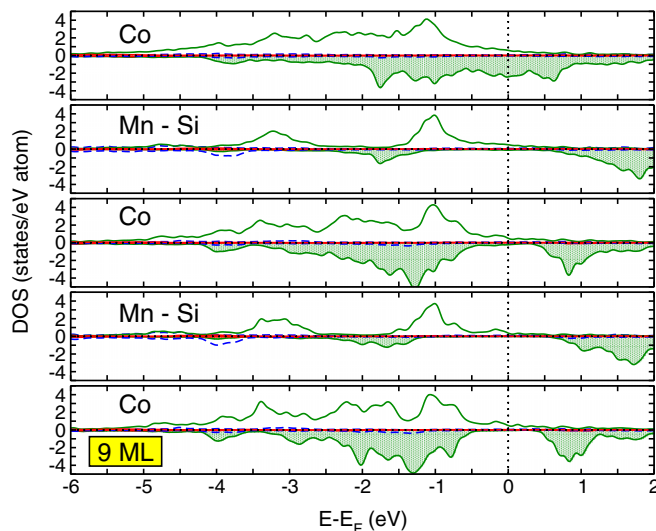
FIG. 24. (Color online) DOS of the Pt-Co$_2$MnSi-Pt system with 9 monolayers of Heusler between the Pt leads.

DOS at the Fermi energy that is mainly associated to the DOS of the Pt leads (see the Appendix where the electronic DOS of the first three layers of the leads are shown). As the states associated with this peak are localized and as in addition there are only very few states within this energy range in the Heusler layer, their contribution to the conductance of the minority channel is only small. Therefore, the DOS of the Heusler layer determines the spin dependence of the conductance almost completely. It shows that the Heusler layer acts as a spin filter even if relativistic effects are taken into account within the calculation of the transport coefficients.

VI. SUMMARY

Theoretical predictions of electronic, magnetic, and thermoelectric properties of half-metallic Heusler alloys have been reported. The half-metallic shape of the DOS of the bulk material is reproduced except for the case of Co$_2$FeSi. This is attributed to the deficient description of the e_g states of Fe which leak into the half-metallic gap.

The calculation of magnetic exchange parameters leads to an accurate reproduction of the experimental trends of the Curie temperatures of Co-based Heusler alloys. The Heisenberg description of the finite-temperature magnetism of the Co-based Heusler alloys is a good choice because the expected thermal fluctuations of the important magnetic

TABLE III. Comparison of the polarization of the conductance and the total electronic density of states of the entire system.

| | Conductance | | DOS | |
	5 ML	9 ML	5 ML	9 ML
Co$_2$FeAl	0.07	0.32	−0.27	−0.27
Co$_2$FeSi	0.18	0.28	−0.25	−0.26
Co$_2$MnAl	0.10	0.28	−0.21	−0.17
Co$_2$MnSi	0.19	0.31	−0.24	−0.20

moments of Co, Mn, and Fe are basically transversal and therefore captured by the MC simulation of the Heisenberg model.

The consistent theoretical results of electronic and finite-temperature magnetic properties clearly indicate the reliability and accuracy of the approach used here. The transport calculations presented here are carried out for the ballistic regime. Therefore, no inelastic scattering of electrons is considered. The temperature dependence enters the calculation only through the derivative of the Fermi function. Therewith, the additional activation of transport channels with increasing temperature is taken into account. Effects of phonons and magnetic excitations are neglected.

The transport calculations show that the Seebeck coefficient strongly depends on the details of the system. Therefore, small changes of the layer thickness and of the composition can result in strong changes of the behavior of the Seebeck coefficient. This allows a precise tuning of the thermoelectric properties.

It can be stated that the Seebeck coefficient does almost solely depend on coarse properties of the energy dependence of the conductance. The main contribution is given by the averaged slope of this property. In particular, a small conductance can lead to large Seebeck coefficient if its slope is large enough.

If the calculated Seebeck coefficients of the composite Pt-Heusler-Pt systems are compared to the experimental measurements of bulk Seebeck coefficients of Co-based Heusler alloys (see Ref. [27]), fundamental differences are observed. The most obvious fact is that all except the nine-layer Co$_2$FeSi and Co$_2$MnSi systems show positive Seebeck coefficients over the whole temperature range. The experimental observation of Seebeck coefficients of the corresponding bulk materials reveals negative values for all systems. It is even more surprising that the composite systems exhibit positive Seebeck coefficients because Pt shows also a negative Seebeck coefficient above 200 K.

It clearly turns out that thin films of half-metallic Heusler alloys between Pt leads give rise to strong spin-polarized currents and in addition to spin-polarized thermoelectric currents. They only need to consist of nine monolayers because from nine monolayers on, half-metallicity is recovered within the Heusler film. This leads to a significant suppression of the conductance of the spin-down channel together with a slope that differs strongly from that of the spin-up channel. This leads to a large difference between both contributions to the total Seebeck coefficient.

The only drawback of this interpretation is the fact that the half-metallicity of Co-based Heusler alloys is strongly temperature dependent. Therefore, the spin polarization in such Heusler alloys is strongly reduced at higher temperatures.

In addition, it should be noted that the choice of the Pt-Co interface between the Pt leads and the Heusler layer has a particular influence on the transport properties. This interface is strongly responsible for the value of the conductance as well as for the degree of spin polarization of the electric current in such systems. Further investigation could include the analysis of interfaces between Pt and Fe-Z and Mn-Z (Z = Al, Si) layers. Such layers can be used on both sides and also the combination of mixed and pure Co layers is of interest. In addition, Pt-based Heusler alloys could be considered in order

to give almost perfect interfaces between lead and Heusler. A systematic analysis of the effect of the interface between Heusler alloys and semiconductors is reported in Ref. [5].

In summary, a consistent theoretical description of Co-based Heusler alloys and Pt-Heusler-Pt composite systems is presented here. In particular, the composite systems have turned out to be promising candidates for the generation of spin-polarized currents by applying a thermal gradient. In future work, the properties of systems with larger Heusler layers have to be carried out, and in addition the k-point resolved density of states needs to be taken into account to give a more detailed insight into the transport mechanisms.

APPENDIX

This appendix is devoted to the electronic structure of the Pt leads of the systems analyzed in Secs. V C and V D. All figures show the first three layers of the Pt leads which are equal on both sides because of the reflection symmetry of the system. This means that the DOS denoted with Pt_1 corresponds to the layer which is directly connected to the Heusler. The DOS denoted with Pt_2 and Pt_3 correspond to the subsequent layers deeper in the lead.

Figure 25 shows the DOS of the Pt leads of the Pt-Co$_2$FeAl-Pt and Pt-Co$_2$FeSi-Pt systems with 5 and 9 monolayers of Heusler. The same is shown in Fig. 26 for the Pt-Co$_2$MnAl-Pt and Pt-Co$_2$MnSi-Pt systems. The main feature which occurs in all systems is the induced magnetization of the first Pt layers of the lead. This can be immediately deduced from the asymmetry of the DOS of the majority and the minority channels. In all cases, the majority DOS of the first layer is small and quite
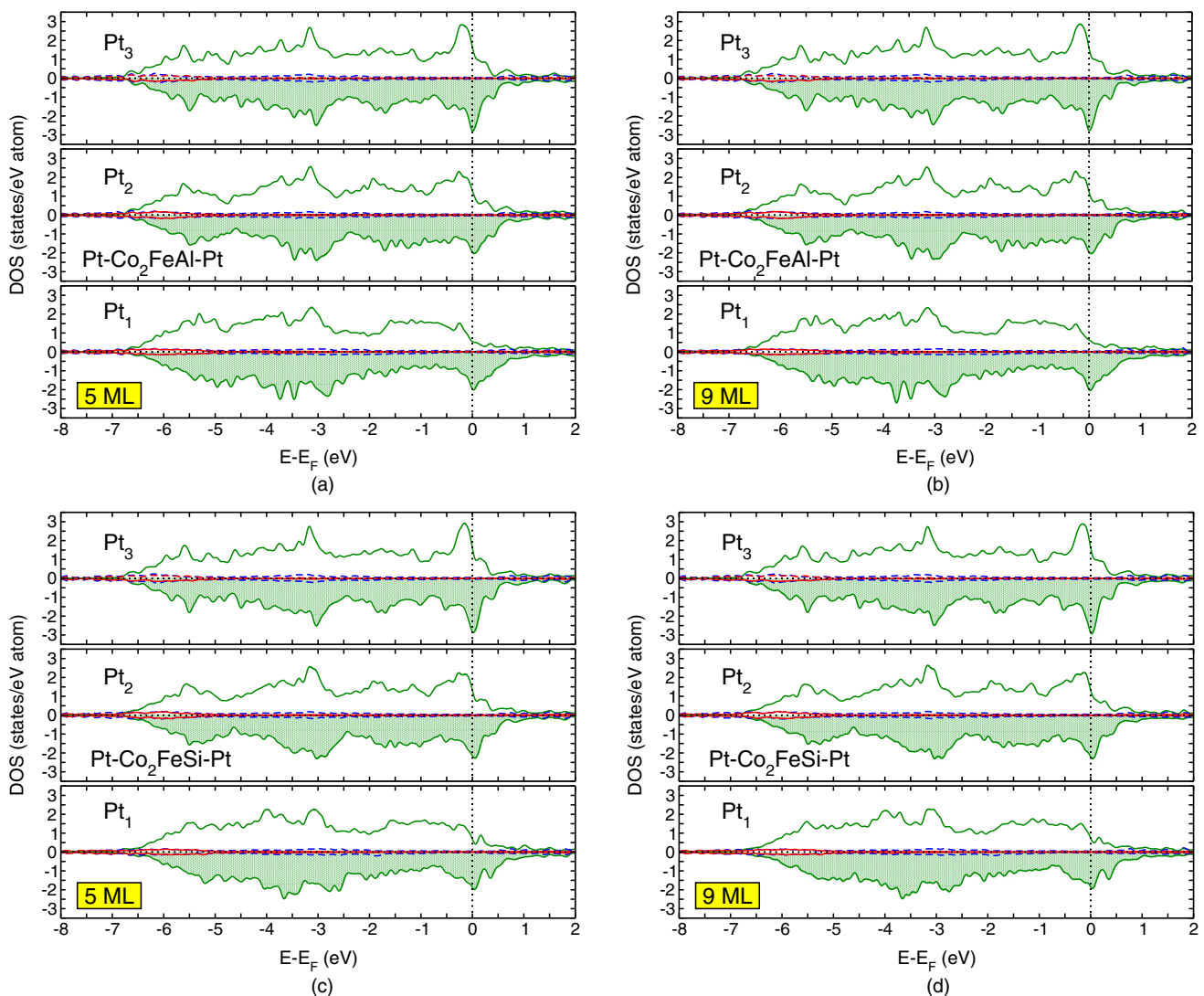

FIG. 25. (Color online) DOS of Pt leads of the Pt-Co$_2$FeAl-Pt and Pt-Co$_2$FeSi-Pt systems with 5 and 9 monolayers of Heusler.
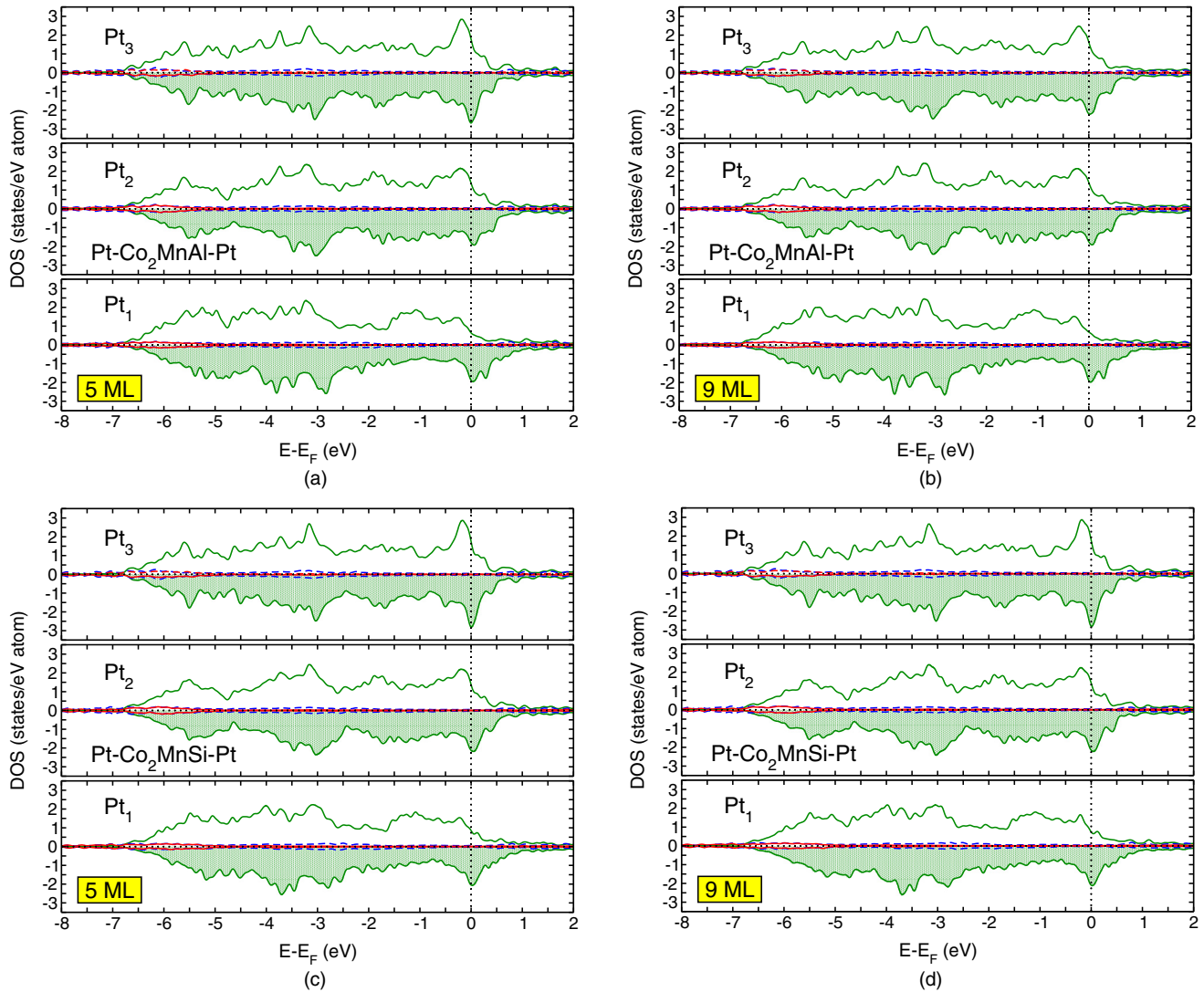
FIG. 26. (Color online) DOS of Pt leads of the Pt-Co$_2$MnAl-Pt and Pt-Co$_2$MnSi-Pt systems with 5 and 9 monolayers of Heusler.

flat at E_F whereas the minority DOS shows a peak. In the subsequent layers, an additional peak in the majority DOS develops. This peak is shifted into the Fermi energy in deeper layers of leads and the DOS becomes that of pure Pt. The DOS of deeper layers is not shown here because the main change is only the shift in the majority channel. The difference in the Pt DOS of systems with 5 and 9 monolayers is very small. Qualitatively speaking, there is no real difference and only some minor quantitative differences occur. In addition, the DOS of the third Pt layer denoted with Pt$_3$ is comparable

for all systems, but especially when comparing the systems including Co$_2$FeAl and Co$_2$FeSi as well as those containing Co$_2$MnAl and Co$_2$MnSi.

Most interestingly, the DOS of the minority channel of the Pt leads is large close to the interface, but the contribution of this channel to the total conductance is smaller in every system considered here (see Table III). Therefore, one can conclude that the Pt states at the Fermi energy are more localized, and the resulting small mobility leads to the small contributions to the conductance.

[1] I. Žutić, J. Fabian, and S. D. Sarma, Rev. Mod. Phys. **76**, 323 (2004).

[2] G. E. W. Bauer, E. Saitoh, and B. J. van Wees, Nat. Mater. **11**, 391 (2012).

[3] A. Slachter, F. L. Bakker, J.-P. Adam, and B. J. van Wees, Nat. Phys. **6**, 879 (2010).

[4] M. I. Katsnelson, V. Y. Irkhin, L. Chioncel, A. I. Lichtenstein, and R. A. de Groot, Rev. Mod. Phys. **80**, 315 (2008).

[5] S. Chadov, T. Graf, K. Chadova, X. Dai, F. Casper, G. H. Fecher, and C. Felser, Phys. Rev. Lett. **107**, 047202 (2011).

[6] L. Gravier, S. Serrano-Guisan, F. Reuse, and J.-P. Ansermet, Phys. Rev. B **73**, 052410 (2006).

[7] V. Popescu and P. Kratzer, Phys. Rev. B **88**, 104425 (2013).

[8] L. Szunyogh, B. Újfalussy, P. Weinberger, and J. Kollár, Phys. Rev. B **49**, 2721 (1994).

[9] S. Lowitzer, D. Ködderitzsch, and H. Ebert, Phys. Rev. B **82**, 140402 (2010).

[10] W. H. Butler, Phys. Rev. B **31**, 3260 (1985).

[11] P. Mavropoulos, N. Papanikolaou, and P. H. Dederichs, Phys. Rev. B **69**, 125104 (2004).

[12] U. Sivan and Y. Imry, Phys. Rev. B **33**, 551 (1986).

[13] S. Wimmer, D. Ködderitzsch, K. Chadova, and H. Ebert, Phys. Rev. B **88**, 201108(R) (2013).

[14] P. Giannozzi, S. Baroni, N. Bonini, M. Calandra, R. Car, C. Cavazzoni, D. Ceresoli, G. L. Chiarotti, M. Cococcioni, I. Dabo *et al.*, J. Phys.: Condens. Matter **21**, 395502 (2009).

[15] J. P. Perdew, K. Burke, and M. Ernzerhof, Phys. Rev. Lett. **77**, 3865 (1996).

[16] H. Ebert, Rep. Prog. Phys. **59**, 1665 (1996).

[17] H. Ebert, in *Lecture Notes in Physics Vol. 535*, edited by H. Dreyssé (Springer, Berlin, 1999), p. 191.

[18] A. I. Liechtenstein, M. I. Katsnelson, and V. A. Gubanov, J. Phys. F: Met. Phys. **14**, L125 (1984).

[19] A. I. Liechtenstein, M. I. Katsnelson, V. P. Antropov, and V. A. Gubanov, J. Magn. Magn. Mater. **67**, 65 (1987).

[20] H. U. Baranger and A. D. Stone, Phys. Rev. B **40**, 8169 (1989).

[21] I. Galanakis, P. H. Dederichs, and N. Papanikolaou, Phys. Rev. B **66**, 174429 (2002).

[22] H. C. Kandpal, G. H. Fecher, C. Felser, and G. Schönhense, Phys. Rev. B **73**, 094422 (2006).

[23] J. Thoene, S. Chadov, G. Fecher, C. Felser, and J. Kübler, J. Phys. D: Appl. Phys. **42**, 084013 (2009).

[24] H. Luo, Q. Hu, C. Li, B. Johansson, L. Vitos, and R. Yang, J. Phys.: Condens. Matter **25**, 156003 (2013).

[25] V. Jung, G. H. Fecher, B. Balke, V. Ksenofontov, and C. Felser, J. Phys. D: Appl. Phys. **42**, 084007 (2009).

[26] I. Galanakis and E. Şaşıoğlu, Appl. Phys. Lett. **98**, 102514 (2011).

[27] B. Balke, S. Ouardi, T. Graf, J. Barth, G. F. Blum, G. H. Fecher, A. Shkabko, A. Weidenkaff, and C. Felser, Solid State Commun. **150**, 529 (2010).